Thermal Evolution of the "Mouse Fur" of Fibrous Aluminium Oxide/Hydroxide Formed on Amalgamated Aluminium upon Reaction with Moist Air

F. Javier García-García, Lorenz Kienle, and Arndt Simon

Max-Planck Institut für Festkörperforschung, Heisenbergstr. 1, D-70569 Stuttgart, Germany

Reprint requests to Dr. F. J. García-García. E-mail: Javier.Garcia@Physik.uni-augsburg.de

Z. Naturforsch. **61b,** 995 – 1001 (2006); received February 16, 2006

Nano-fibres of amorphous aluminium oxide/hydroxide have been obtained *via* reaction of amalgamated aluminium with moist air. Thermal transformation of the as prepared sample was followed by X-ray powder diffraction and electron microscopy techniques. Crystallisation of γ-Al_2O_3 nanocrystals inside the amorphous fibres starts at 400 °C and the maximum crystal size is achieved at 700 – 800 °C. The fibrous transition alumina matrix transforms into a sponge-like morphology between 800 and 900 °C. Annealing at higher temperature results in the condensation into large globular α-Al_2O_3 crystals. The entire γ- to α-Al_2O_3 transformation occurs *via* two consecutive steps of coalescence and explosive character, respectively. The direct contact between transition alumina crystals governs the transformation. The presence of some other transition alumina is inferred from high resolution electron microscopy studies, and antiphase boundaries in {111} of the spinel type structure for γ-Al_2O_3 obviously determine the crystallographic path between them.

Key words: Fibrous Amorphous Aluminium Oxide/Hydroxide, Thermal Evolution, Phase Transformation, Electron Microscopy, Powder X-Ray Diffraction

Introduction

A "mouse fur" of fibrous aluminium oxide/hydroxide forms on amalgamated aluminium upon reaction with air. The product of this long known reaction [1] was reported to be γ-Al_2O_3 (spinel type structure) [2], and it adds to the manifold of "transition aluminas" [3]. The present study is devoted to the characterisation *via* X-ray powder diffraction and transmission electron microscopy techniques of the nano-fibrous aluminium oxide/hydroxide produced in this way. This investigation follows its thermal transformation into other transition aluminas and finally into α-Al_2O_3 (corundum type structure). Some reports in the literature addressed this subject, however, with different starting materials than the one used here, *e. g.* [4, 5].

Transition aluminas have been extensively studied over the last decades [6], owing to their large surface area and porosity. They adopt intrinsically disordered structures, and samples are poorly crystalline. Furthermore, synthetic method and chemical history of the starting materials show a strong influence both in the intermediate transition sequence and in the final product. In the present case, the successive formation of γ-, σ-, θ- and α-Al_2O_3 is expected when the starting material is heat treated [3]. This sequence coincides with that obtained when boehmite is thermally dehydrated, and it has been thoroughly studied [7, 8] as it is the traditional route for synthetising the industrially used γ-Al_2O_3. Therefore, a parallel investigation by using boehmite as starting material was performed for comparison.

Experimental Section

An Al foil was treated with concentrated HCl, quickly rinsed with distilled H_2O and then wetted with Hg. In contact with air the formation of a light grey fur of fibrous alumina is fast enough to see it growing to several millimetres thickness within minutes. Boehmite was precipitated from a solution of $Al(NO_3)_3$ in H_2O which was brought to pH = 8 to 9 by adding aqueous NH_3 dropwise. The precipitate was filtered, washed with distilled H_2O three times and dried at 50 °C while stirred. This latter procedure was repeated by subsequent suspension of the product in fresh H_2O.

Samples were annealed in air at temperatures from 200 to 1200 °C in steps of 100 °C. Annealing time was selected by following statements in literature [2] that reactions are completed after 48 h. Much shorter times, 30 min, were also chosen in order to capture transient phases. Two series of samples resulted, namely Series I (fibrous alumina) and Se-

ries II (boehmite). In what follows they are correspondingly referred to in the text.

For X-ray powder diffraction the samples were mounted in 0.3 mm glass capillaries, and data collections were carried out in a STOE powder diffractometer (Cu-$K_{\alpha 1}$, Ge monochromator). The software PowderCell [9] was used for evaluation of the data. Specimens for electron microscopy were prepared by ultrasonic dispersion of the samples in butanol. A drop of the resulting suspension was put onto a holey carbon-coated copper grid. The investigation was performed on a Philips CM30ST microscope operated at 300 kV.

Results

X-ray diffraction

Series I: Fibrous alumina

X-ray diffraction patterns of samples annealed at different temperatures are presented in Fig. 1a. The as-prepared sample is completely amorphous. A very weak reflection develops at 400 to 500 °C which can be indexed as 440 of γ-Al_2O_3. In the 700 °C sample the most pronounced diffuse maxima, at $2\theta \approx 45.5°$($d \approx 0.198$ nm) and $2\theta \approx 66.5°$($d \approx 0.140$ nm), might correspond to the 400 and 440 reflections of γ-Al_2O_3. In addition to these bumps, weak sharp reflections from α-Al_2O_3 appear at 900 °C which becomes the only present phase at 1100 °C and above. Prolonged heating at 1000 °C for 96 h results in a complete absence of γ-Al_2O_3. Shorter annealing periods do not produce evidence for any other phases than γ- and α-Al_2O_3. The characteristic 400 and 440 maxima of the γ-phase are seen after 4 h at 700 °C, and 30 min are sufficient to produce the single phase diagram of α-Al_2O_3 at 1200 °C. The refined unit cell parameters for this phase are $a = 4.754(9)$ and $c = 12.970(14)$ Å.

Quantification of the average particle size by using the Scherrer equation [10] might be misleading due to omission of strain. However, as crystallisation takes place within an amorphous matrix such a simplification should be allowed. Using the close-lying reflections of α-Al_2O_3, formed at 1200 °C, to estimate the instrumental broadening, we derive particle sizes of approx. 12 nm for samples prepared at 700 to 900 °C and slightly less, approx. 8 nm, at 600 °C. Reflections from the α-Al_2O_3 phase do not experience broadening from crystal size effect. Single broad diffraction peaks in the low angle regions of the diffraction patterns are present in samples annealed up to 1000 °C. They denote the presence of a disordered mesoporous structure with an

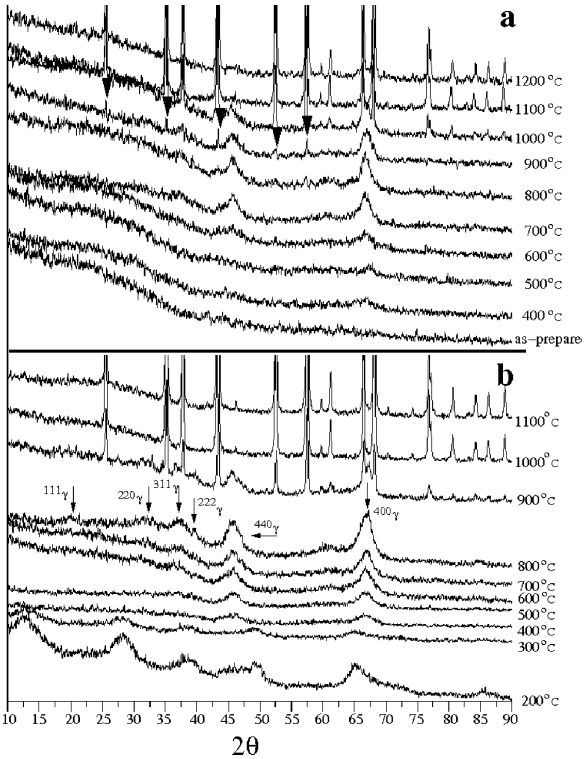

Fig. 1. X-ray powder diffraction patterns of annealed samples from series I, fibrous alumina, and series II, boehmite, are presented in (a) and (b), respectively. The annealing temperatures, for 24 h, are indicated.

average inter-pores spacing of approx. 6 nm. Such a result is typical in transition aluminas synthetized by dehydration of boehmite [11].

Series II: boehmite

Fig. 1b presents the X-ray diagrams of samples annealed at the given temperatures. The typical pattern for nanosized crystals of boehmite is seen for the 200 and 300 °C samples. At 400 °C it changes to that of γ-Al_2O_3 with diffuse maxima for the 400 and 440 reflections. This structure develops further, and at 800 °C some more reflections, as indexed in Fig. 1b, are present. After annealing at 1000 °C and higher, only the pattern of α-Al_2O_3 is left. Again, the time dependence of the pattern evolution is quite significant, however, with no evidence for additional phases. In the 200 to 800 °C range, 4 to 6 h are needed to produce the diagrams shown in Fig. 1b. After 30 min at 900 °C the broad 400 and 440 reflections of the γ-Al_2O_3 are seen, and after 16 h all reflections of α-Al_2O_3 are present. The particle size for the boehmite crystals in

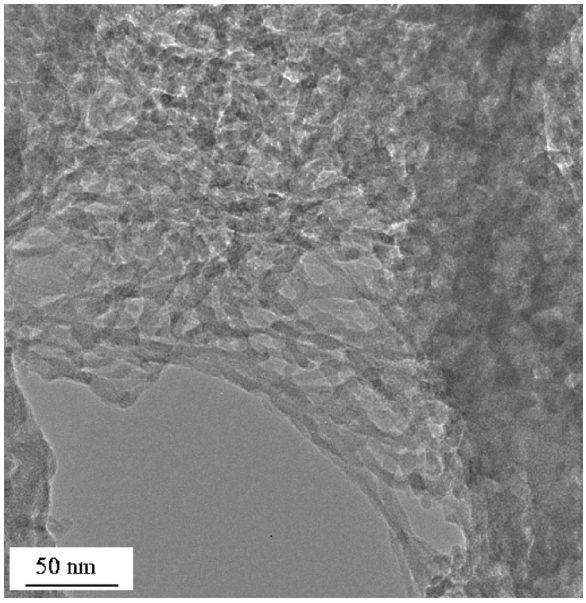

Fig. 2. Transmission electron microscopy image of a typical as-prepared sample from series I, fibrous alumina. The particles are composed of fibres of amorphous aluminium oxide/hydroxide.

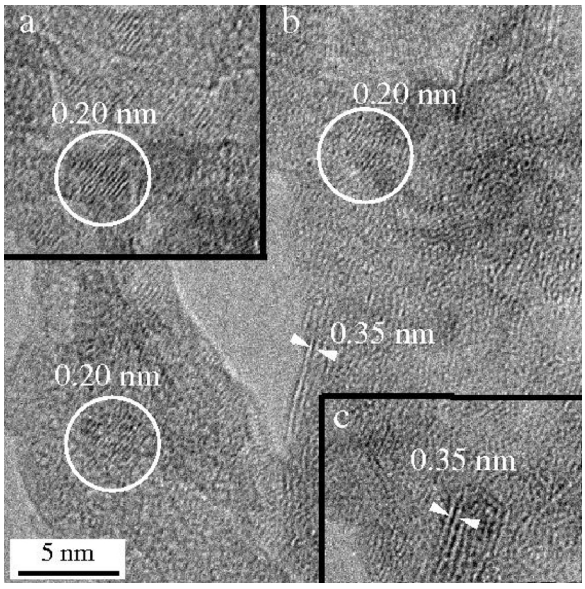

Fig. 3. In (a), (b) and (c) high resolution images of three different areas taken in a particle of the samples from series I, fibrous alumina, annealed at 400 and 500 °C during 24 h are presented. Some nano-crystals embedded in the amorphous matrix are encircled. The measured periodicities are indicated.

the 200 °C samples estimated from the low-angle maxima, 020 and 120, respectively, is ≈ 5 nm. The particle sizes for γ-Al_2O_3 are slightly different from those in series I, namely 10, 8 and 7 nm for 800 °C, 700 °C and 600 °C, respectively.

Electron microscopy

The investigation in the transmission electron microscope shows that the as-prepared sample of series I (fibrous alumina) is composed of nanosized fibres, see Fig. 2. They are completely amorphous, and no *in-situ* crystallisation was observed while keeping the fibres in the beam of electrons, in contrast to results reported in [12]. Therefore, the results described in the following reflect the effects of *ex-situ* thermal treatments.

The samples of series I treated at 400 and 500 °C show crystalline inclusions, of a size well below 5 nm, within the fibres, see Fig. 3. The periodicity measured, $d \approx 0.20$ nm, could correspond to the 400 reflections of the γ-Al_2O_3 which is clearly observed as a slightly diffuse ring in the electron diffraction patterns. In addition, Fig. 3b shows fringes with a periodicity of $d \approx 0.35$ nm on the fibres surfaces, indicated by arrow heads. A needle-like particle exhibiting these fringes is shown in Fig. 3c. Its origin remains unclear, as it does not correspond to any spacing of γ-Al_2O_3. A possible explanation might be given based on surface reconstruction or relaxation [13]. Annealing at higher temperature leads to crystallisation of larger parts of the fibres and changes of their morphology. Two images at different magnification of the sample heated at 800 °C are shown in Figs. 4a and b. The imaged fibres are composed of nano-crystallites characterised by straight surfaces and facets. The fringes with a spacing of $d \approx 0.46$ nm might correspond to (111) of γ-Al_2O_3. Areas of amorphous starting material are still present and fringes with $d \approx 0.35$ nm as in Fig. 3 are rarely observed. Figs. 4c and 4d present the images of spherical crystalline particles found in this sample. The periodicity of 0.36 nm comes close to the corresponding one for the (111) in α-Al_2O_3 (Fig. 4c), whereas fringes with $d \approx 0.204$ nm occur with the particle in Fig. 4d (to help the eye, the digital diffraction pattern is inset). The observed d value could also be assigned to 400 of γ-Al_2O_3, however, with respect to the interpretation of Fig. 4c, an indexing with 113 of α-Al_2O_3 seems more reasonable. An image of the large and well ordered α-Al_2O_3 crystals formed at 1000 °C is shown in Fig. 5a, and in 5b an image of a transition alumina

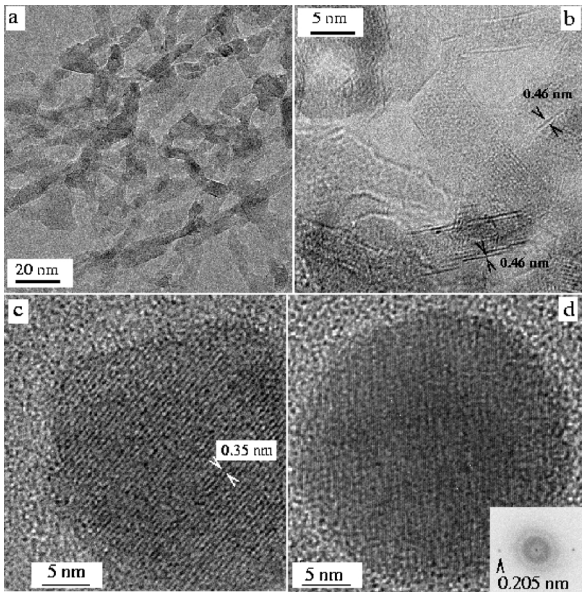

Fig. 4. In (a) and (b) two high resolution images of the 800 °C sample from Series I, fibrous alumina, are shown. Note the differences in the shape of the fibers in comparison with Fig. 1. On the surface of the fibers fringes of ≈ 0.46 nm are observed and arrowed in the picture. In (c) and (d), we present the images of two isolated spherical α-Al_2O_3 crystals in the 800 °C sample from Series I, fibrous alumina. The observed periodicities are indicated. In (d) the Fourier transform is inserted to help the eye.

particle in this sample is presented. The globular character of the crystallites as well as the holes in their centres (arrowed in the picture) are eye-catching features, and they suggest some kind of coalescence between crystals as those seen in Figs. 4c and 4d. The particles shown in Fig. 5b present a sponge-like morphology where the fibres have disappeared. For comparison, Figs. 6a and 6b present images of a particle from series I annealed at 800 °C and of a particle from series II annealed at 600 °C, respectively. The latter exhibits a granular structure composed of γ-Al_2O_3 nanocrystals and thoroughly differs from the morphology in 6a which preserve the fibre character still at 800 °C. Note the similarities between Figs. 5b and 6b.

Discussion

Particle size

In samples from Series I the γ-Al_2O_3 crystals achieve the size of the fibres, approx. 12 nm, at ≈ 700 °C. The transformation to α-Al_2O_3 starts at ≈ 900 °C and is completed at ≈ 1000 °C. In the temperature range between 700 to 900 °C a fibrous to sponge-like particle transformation occurs. In contrast, smaller crystals, ≈ 10 nm, are observed in samples from series II prior to the formation of the α-Al_2O_3 which occurs at ≈ 900 °C. These experimental results suggest that the transition into α-Al_2O_3 is independent of the γ-Al_2O_3 crystal size but ruled by the physical contact between the transition alumina crystals. Crystals embedded in a sponge-like matrix experience intimate contact between themselves and the subsequent condensation of α-Al_2O_3 is favoured. The temperature for the final transformation into α-Al_2O_3 is different by ≈ 100 °C between series I and II. We attribute such a difference to the morphological transformation in the transition alumina particles prior to the final transition into α-Al_2O_3.

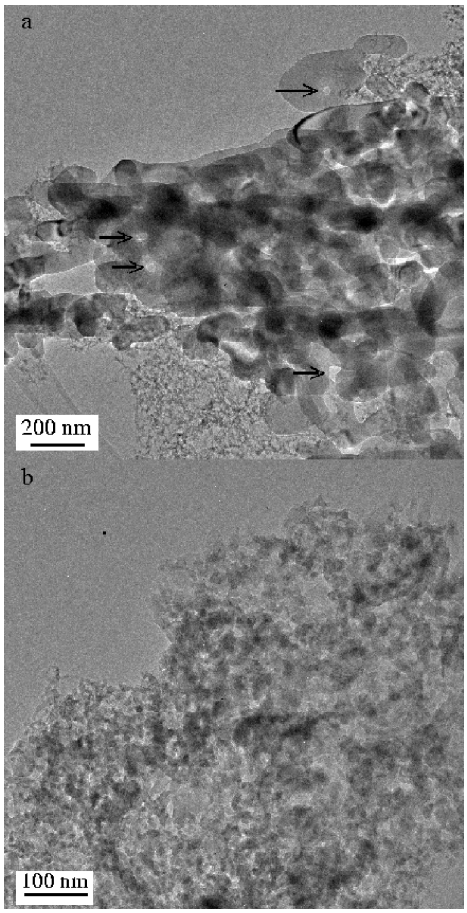

Fig. 5. In (a) an image showing the typical α-Al_2O_3 crystals in the 900 °C sample from Series I, fibrous alumina, is presented. An image of the remaining transition alumina matrix is shown in (b). Compare with Fig. 3.

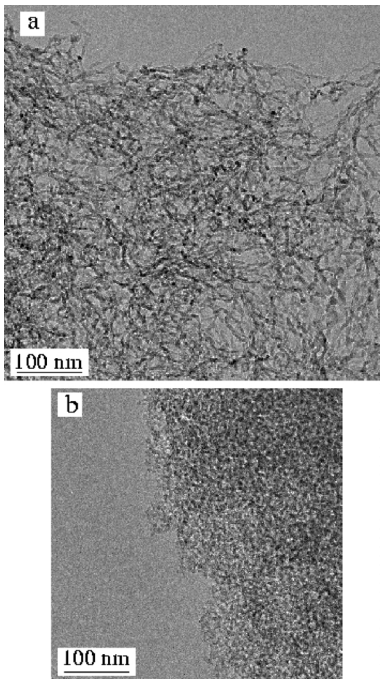

Fig. 6. The γ-Al_2O_3 particles matrix in the 800 °C in samples from Series I, fibrous alumina, and in the 600 °C samples from Series II, boehmite, are presented in (a) and (b) respectively. Note the apparent morphological difference.

α-Al_2O_3 growth mechanism

In the Series I samples the spherically shaped α-Al_2O_3 crystals formed at $\approx$ 900 °C double the size of the parent γ-Al_2O_3 crystals. Several of these crystals coming together might well explain the globular shape of the α-Al_2O_3 crystals, as well as the holes, observed at higher annealing temperature. Structural defects in these crystals could not be observed even at the junctions between formerly different α-Al_2O_3 crystals. Thus, the entire γ to α transition is divided into two consecutive coalescence processes. In a first step the γ- to α-phase transition occurs, and in the second one some of these crystals coalesce giving rise to larger α-Al_2O_3 crystals. Such a result is in agreement with the findings reported in [14]. Additionally, explosive grain growth was also suggested in the same reference and might well also be adopted in the present case. In order to further understand these processes we might take into account the effect of particle size. In the present samples it is well below 15 nm, which is the calculated critical value for stability of the γ-Al_2O_3 phase [15]. With this data at hand, it is easy to imagine that whenever two or more of the γ-Al_2O_3 crystals get into direct contact, the thermodynamic stability of α-Al_2O_3 is spontaneously achieved and the transformation occurs explosively.

Structural disorder

The structure of γ-Al_2O_3 is related to the spinel structure type [16]. Al is partially, and almost randomly, filling the octahedral and tetrahedral sites of a well ordered cubic close packed array of oxygen atoms. Such a model of disorder is suggested for our samples, as the most prominent observed reflections, 440 and 400, are due to scattering from the anion substructure in the case of the ideal spinel type structure. Only the corresponding diffraction rings for these two reflections are clearly observed in the electron diffraction patterns. Reflections with only contribution from the cation substructure are completely absent in the X-ray diffraction patterns and just occasionally observed, as faint rings, in the electron diffraction experiments. Thus, we might refer to a strongly disordered cation substructure in a rather well ordered substructure of the anions. The samples from series II (boehmite) annealed at 800 °C deviate from this tendency as some more reflections at lower diffraction angles appear in the X-ray powder pattern.

Crystal chemistry

Only faint indications of the presence of intermediate transition alumina phases could be detected. The high resolution images presented in Figs. 7a, c and e were recorded on different crystals of the sample from series I annealed at 900 °C. The corresponding Fourier transforms are shown in Figs. 7b, d, and f, respectively. The set of directions $\langle 111 \rangle^*$ of the basic spinel type structure is in common, and the 111 reflection is well defined in (b), but rather diffuse in (d), and in (f) it is accompanied by weak satellite reflections, arrowed in the picture. In contrast, no differences are observed for the 222 reflection. Note that in the present case these differences are fully independent of thickness and/or defocus conditions in the electron microscope. The 111 and 222 reflections owe their intensity to scattering from the cation and anion sublattices, respectively. Thus, the differences in the 111 reflection might be explained as due to different partial order in the disordered cation substructure whilst the anion substructure remains unchanged. Further, there ex-

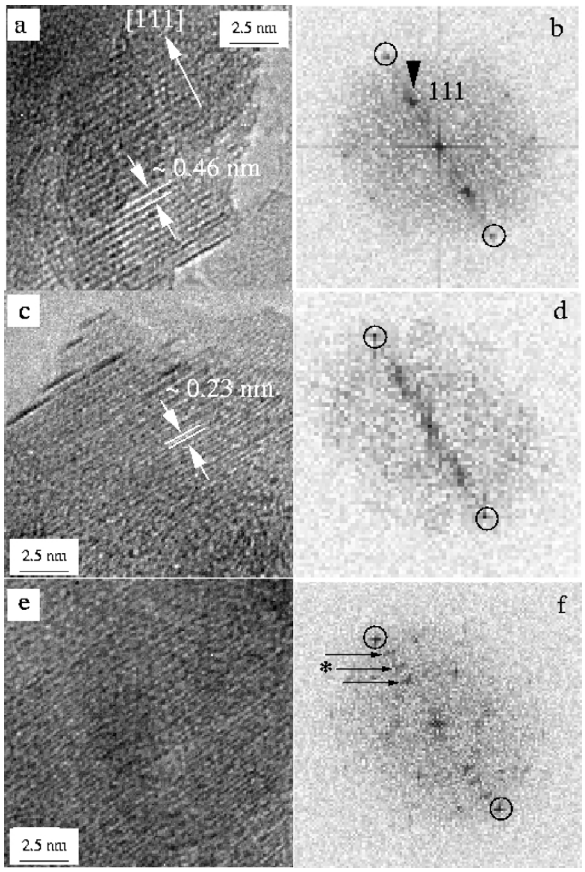

Fig. 7. In (a), (c) and (e) high resolution images of three different crystals of the γ-Al_2O_3 structure are presented. The images were recorded in the sample from series I annealed at 900 °C. The corresponding Fourier transforms are shown in (b), (d) and (f), respectively. The common maxima, indexable as 222, are encircled. Note the differently shaped reflections for 111, which is interpreted as due to disorder in the cation substructure.

ists some kind of superstructural ordering along $[111]^*$, see f. All these results are in agreement with the findings reported in [17], where all phase transformations were reported to happen along different ordered patterns of aluminium atoms in the interstitial sites of the cubic close packed array of oxygen atoms. Therein, a new transition alumina, the so-called θ', was reported to condense out as a result of (cation) ordering along $[111]^*$. The coincidence in the superstructure direction suggests that the superstructural principle behind these reflections might be similar. In favour of such an assumption is the fact that the satellite indicated by an asterisk in Fig. 7f exactly corresponds to $2/3[111]^*$, as reported in [17].

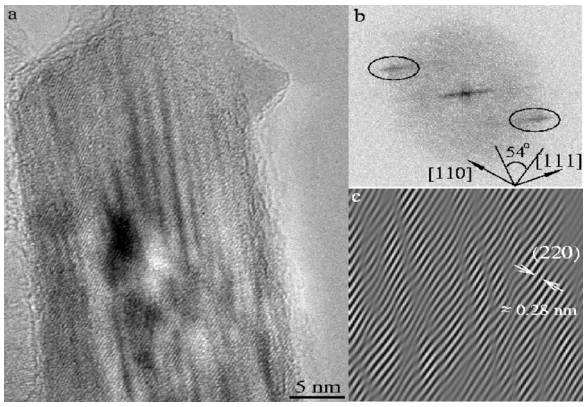

Fig. 8. In (a) and (b) a high resolution image of a γ-Al_2O_3 crystal and the corresponding Fourier transforms are presented, respectively. The image presented in (c) is the inverse Fast Fourier transform of (b) and the areas used for the masking process are encircled in (b). The calculated $\{111\}$ of the spinel type structure is shown as an inset in (b).

Interestingly, and in marked contrast to this result, superstructural ordering along $\langle 110 \rangle$ has also been experimentally observed [6, 18]. A high resolution image of a different crystal in the same sample is presented in Fig. 8a. The corresponding Fourier transform is shown in Fig. 8b, where the areas used for the inverse Fourier transformation, presented in 8c, are encircled. The image in 8c is composed of domains of parallel stripes at a constant distance of ≈ 0.28 nm; they are accordingly interpreted as derived from the 220 reflections of γ-Al_2O_3. The narrow areas between these domains correspond to the introduction of anti-phase boundaries between two consecutive domains. The inset in Fig. 8b shows the calculated $\langle 111 \rangle^*$ by using the observed fringes from $[110]^*$, in 8c, along with the theoretical angle of $\approx 54^\circ$ between these two directions. The rods of streaking in the digital diffraction pattern are rather close to $\langle 111 \rangle^*$ and, hence, the antiphase boundaries are lying in $\{111\}$ of the cubic spinel structure and not in $\{110\}$, in agreement with the results from Fig. 7.

Finally, we would like to point out that the proposed coalescence and explosive grain growth make the search for possible transformation paths from transition aluminas to α-Al_2O_3 obsolete.

Conclusions

The grey fibrous "mouse fur" formed on amalgamated aluminium in contact with moist air is composed of nanofibres of amorphous aluminium ox-

ide/hydroxide. Annealing in air at 400 °C leads to the crystallisation of γ-Al_2O_3 nanocrystals inside the fibres. These crystals grow up to a maximum size given by the diameter of the fibres, which is achieved at 700 – 800 °C. At this point the fibres break and the resulting crystalline fragments, as well as some remaining amorphous material, come together to form granular particles. The surface contact between neighbouring transition alumina crystals increases, and they coalesce to form α-Al_2O_3 spherical crystals. The large globular α-Al_2O_3 crystals are formed after a second (explosive) coalescence process.

The presence of some other transition aluminas is inferred from the high resolution electron microscopy studies. Our results are in full agreement with the previously reported studies on the subject, somewhat obscured due to the observed crystal size and strong disorder. However, the formation of antiphase boundaries in $\{111\}$ of the spinel structure seems to be the crystallographic path between different transition aluminas.

[1] H. Wislicenus, Kolloid-Z **2**, 11 (1908).
[2] M. R. Pinnel, J. E. Bennet, J. Mater. Sci. **7**, 1016 (1972).
[3] I. Levin, D. Brandon, J. Am. Ceram. Soc. **81**, 1995 (1998).
[4] T. C. Chou, T. G. Nieh, J. Am. Ceram. Soc. **74**, 2270 (1991).
[5] F. W. Dynys, J. W. Halloran, J. Am. Ceram. Soc. **65**, 442 (1991).
[6] B. C. Lippens, J. H. de Boer, Acta Crystallogr. **17**, 1312 (1964).
[7] R. W. Hicks, T. J. Pinnavaia, Chem. Mater. **15**, 78 (2003).
[8] M. L. Guzmán-Castillo, X. Bokhimi, A. Toledo-Antonio, J. Salmones-Blásquez, F. Hernández-Beltrán, J. Phys. Chem. B **105**, 2099 (2001).
[9] W. Kraus, G. Nolze, J. Appl. Crystallogr. **29**, 301 (1996).
[10] D. B. Cullity, Elements of X-ray Diffraction, Addison-Wesley, London (1956).
[11] Z. Zhang, R. W. Hicks, T. R. Pauly, T. J. Pinnavaia, J. Am. Chem. Soc. **124**, 1592 (2002).
[12] A. J. Bourdillon, S. M. El-Mashri, A. J. Forty, Phil. Mag. A **49**, 341 (1983).
[13] S. Blonski, S. H. Garofalini, Surface Science **295**, 263 (1993).
[14] T. C. Chou, T. G. Nieh, J. Am. Ceram. Soc. **74** 2270 (1991).
[15] J. M. McHale, A. Auroux, A. J. Perrota, A. Navrostky Science **277**, 788 (1997).
[16] R. S. Zhou, R. L. Snyder, Acta Crystallogr. **B47**, 617 (1991).
[17] I. Levin, L. A. Bendersky, D. G. Brandon, M. Rühle, Acta Mater. **45**, 3659 (1997).
[18] T. C. Chou, T. G. Nieh, J. Am. Ceram. Soc. **74**, 2270 (1991).